Journal of Energy Storage 168 (2026) 122655

Contents lists available at ScienceDirect

Journal of Energy Storage

journal homepage: www.elsevier.com/locate/est

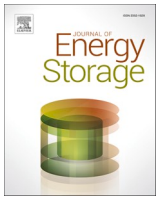

Research papers

Data-driven discovery of dynamic thermodynamics for dehydrogenation in magnesium-based hydrogen storage materials

Jianghao Cai [a,b], Yutian Zhuang [a,b], Kang Ma [a,b], Yutong Jiang [a,b], Xuao Lu [a,b], Zhengyang Gao [a,b], Weijie Yang [a,b,*]

[a] School of Energy, Power and Mechanical Engineering, Department of Power Engineering, North China Electric Power University, Baoding, 071003, China
[b] Hebei Key Laboratory of Energy Storage Technology and Integrated Energy Utilization, North China Electric Power University, Baoding, 071003, China

ARTICLE INFO

Keywords:
Mg-based hydrogen storage materials
Dehydrogenation mechanism
Pressure-composition-temperature curves
Dynamic reaction enthalpy
Thermodynamic-kinetic coupling

ABSTRACT

Mg-based hydrogen storage materials often exhibit non-ideal pressure-composition-temperature (PCT) plateaus and multistage transformations during dehydrogenation, which limits the representativeness of conventional single-valued thermodynamic descriptors. This study develops a progress-resolved thermodynamic inversion framework to extract dynamic reaction enthalpy from equilibrium information embedded in PCT curves. Two complementary reconstruction routes are implemented for validation, including a polynomial baseline for empirical curve reconstruction and a thermodynamics-based route that reconstructs PCT behavior by introducing stage-specific dynamic reaction enthalpy into the Van't Hoff relation. The latter better preserves non-ideal plateau morphology and progress-dependent turning behavior. A literature-scale compilation covering pure MgH_2, catalyst-modified MgH_2 composites, and Mg-based alloys reveals statistically comparable dynamic reaction enthalpy trajectories on a unified normalized progress axis. The mean within-material spans reach 20.60, 24.70, and 24.00 kJ/mol for the three material classes, respectively, indicating substantial progress-dependent thermodynamic heterogeneity. Global thermodynamic verification further shows that the maximum absolute differences between the global average reaction enthalpy and the reference plateau reaction enthalpy are 4.03, 15.29, and 16.52 kJ/mol, respectively, demonstrating pronounced system-dependent dispersion. On a unified progress axis, dynamic reaction enthalpy co-varies with dynamic apparent activation energy with aligned turning positions, supporting a stage-structured framework spanning early interface establishment, mid-progress plateau-governed two-phase transformation, and late-stage active-phase depletion. Overall, this work transforms PCT thermodynamics from a single-value description into a progress-resolved and comparable representation, and provides a stage-aware thermal descriptor for heat-duty estimation, heating power allocation, and dynamic thermal management in practical dehydrogenation reactors.

1. Introduction

Magnesium-based hydrides are among the most intensively investigated materials in solid-state hydrogen storage, owing to their high theoretical capacity, elemental abundance, and low cost, which make them attractive for scalable and application oriented hydrogen storage and supply modules [1–3]. However, their practical dehydrogenation is constrained by the intrinsically high thermodynamic stability of MgH_2 and the concomitantly slow kinetics, which translate into elevated operating temperatures, limited dehydrogenation rates, and reduced system-level energy efficiency [4]. To tackle these coupled constraints, alloying, nano-structuring, and the introduction of efficient catalysts have been extensively explored to accelerate interfacial dissociation and bulk diffusion while tuning the effective stability of the hydride, thereby improving the overall dehydrogenation behavior of Mg-based systems [5,6].

In catalytic strategies, Nb_2O_5-based MOF composites promote hydrogen dissociation at Lewis-acid sites and facilitate mass transport through MOF channels, thereby lowering the onset desorption temperature and reducing the activation energy [7]. Ti_3C_2 (MXene)-supported MnO_2 forms multiphase interfaces with MgH_2, thereby lowering the dehydrogenation onset temperature and enhancing hydrogen storage

* Corresponding author at: School of Energy, Power and Mechanical Engineering, Department of Power Engineering, North China Electric Power University, Baoding, 071003, China.
E-mail address: yangwj@ncepu.edu.cn (W. Yang).

https://doi.org/10.1016/j.est.2026.122655
Received 23 January 2026; Received in revised form 12 April 2026; Accepted 10 May 2026
Available online 13 May 2026

performance [8]. FeCoNiCrTi high entropy nanosheets introduce defect-rich interfaces and accelerate hydrogen diffusion, decreasing the main desorption peak and weakening the stability of Mg—H bonding [9]. The catalytic centers composed of metallic and oxidized FeNiCu phases further enhance interfacial activity and continuously improve the desorption kinetics over the relevant temperature range [10]. Collectively, these catalytic systems weaken Mg—H bonding through multi-metal electronic modulation and reduce the thermodynamic stability of the hydride. In alloying strategies, introducing Ni into $Mg_{85}Zn_6Y_9$ produces Mg_2Ni phases in situ and decreases the activation energy [11]. In nanoscale engineering, Mg nanocrystals shorten the diffusion length and reduce the activation energy [12]. Nanoporous Mg with interconnected channels decreases the dehydrogenation activation energy and lowers thermodynamic stability during dehydrogenation, thereby improving dehydrogenation kinetics [13]. Therefore, size effects primarily accelerate diffusion kinetics, whereas pore channel effects enhance interfacial hydrogen dissociation. Catalytic modification, alloying and nano-structuring improve the desorption behavior of MgH_2 through distinct kinetic pathways. Despite these macroscopic improvements, a systematic understanding of the microscopic, progress-dependent co-evolution of kinetics, thermodynamics, and structure during dehydrogenation remains lacking.

In situ nanoscale observations have revealed that during hydrogen absorption in Mg, hydrogen preferentially adsorbs and dissociates at grain boundaries and defected regions and then propagates into grain interiors along defect networks. In the subsequent dehydrogenation of MgH_2, hydrogen recombination and release likewise initiate at these interfacial sites, thereby exhibiting pronounced kinetic evolution [14]. Density functional theory calculations further demonstrate that grain boundary configurations lower the adsorption and dissociation barriers of hydrogen molecules, reflecting intrinsic interfacial regulation during hydrogenation [15]. Meanwhile, investigations on mechanochemically processed Mg-based composites indicate that hydrogen absorption preferentially proceeds in defect enriched regions and consequently accelerates activation and hydrogenation kinetics [16]. The interfacial studies mainly revealed the boundary initiated nature of hydrogen storage and release, whereas subsequent investigations provided quantitative kinetic relations. Computational results show that the activation barriers of MgH_2 dehydrogenation decrease from the surface to the subsequent layers, displaying a rapid initial drop followed by gradual leveling off along the reaction progress [17]. This progressive release of activation barriers from the surface toward the interior is accordingly termed the “burst effect”. Subsequently, further work employed data-driven kinetic modeling and constructed continuously evolving layer resolved kinetic descriptors to quantify the dynamic variation of dehydrogenation activation barriers along the reaction progress [18]. At the experimental scale, an improved Johnson-Mehl-Avrami-Kolmogorov (JMAK) dynamic kinetic model was established from extensive MgH_2 dehydrogenation curves to reconstruct the evolution of activation energy along the reaction progress, thereby further verifying the burst effect [19]. Building upon these findings, later investigations proposed a demand driven dynamic heating strategy, which matches the energy supply with the evolving barriers along the reaction progress and thus enables faster and more energy efficient MgH_2 dehydrogenation [20].

Thermodynamically, recent studies have begun to treat reaction enthalpy as progress dependent quantities rather than single constants. In metal hydride refrigerant alloys, the desorption enthalpy decreases with increasing hydrogen concentration, as shown by $La_{0.9}Ce_{0.1}Ni_5$ (29.8 to 27.4 kJ/mol over 0.2 wt% to 1.4 wt%) and $LaNi_{4.7}Al_{0.3}$ (29.2 to 27.8 kJ/mol over 0.2 wt% to 1.2 wt%) [21]. In a Ti-based AB2 alloy, the relative partial molar enthalpy also varies with reaction progress, for instance increasing from 12.7 to 13.0 kJ/mol as r rises from 1.6 to 1.8 [22]. For a multi-component AB5 alloy, the thermodynamics of dissolved hydrogen are further analyzed as functions of hydrogen concentration, together with resistance variations that track the evolving state [23]. Collectively, these results show that reaction heat exhibits an intrinsic dynamic signature along the reaction progress, with enthalpy shifting with extent of reaction or hydrogen content. Nevertheless, for magnesium-based solid-state hydrogen storage materials, comparable progress-resolved quantification of dehydrogenation enthalpy or reaction heat remains largely unavailable. Meanwhile, the Brønsted-Evans-Polanyi (BEP) relation states that for mechanistically related reactions the apparent activation barrier often scales approximately linearly with the reaction enthalpy, providing a thermodynamic basis for thermodynamic-kinetic coupling [24,25]. Accordingly, systematic studies that couple kinetics and thermodynamics for Mg-based hydrogen storage materials are still lacking.

To address these issues, this study develops a progress-resolved thermodynamic inversion framework to extract dynamic reaction enthalpy from the equilibrium information embedded in PCT curves and to clarify its operational meaning relative to state-function enthalpy. Two complementary reconstruction routes are implemented to benchmark internal consistency and practical applicability. The validated workflow is then applied to a literature dataset covering pure MgH_2, catalyst-modified MgH_2 composites, and Mg-based alloys, thereby establishing a statistically comparable spectrum of dynamic reaction enthalpy along normalized reaction progress. Global thermodynamic verification is further performed by comparing the globally averaged enthalpy with literature-reported values, and system-dependent differences are interpreted in terms of non-ideal plateau behavior and transformation complexity. Finally, the co-evolution of dynamic reaction enthalpy and dynamic apparent activation energy is examined on a unified progress axis, supporting a stage-structured mechanistic framework and highlighting the engineering relevance of progress-dependent thermodynamic heterogeneity.

2. Model construction and method

Dehydrogenation studies of Mg-based hydrogen storage materials published between 2015 and 2025 were systematically collected to enable data-driven characterization of progress-resolved thermodynamic features. All data are sourced from the Digital Platform for Solid-State Hydrogen Storage (*Digital Hydrogen-S)* (http://digital-hydrogen.com/storage/index-white.html) [5]. The dataset covers pure MgH_2, catalyst-modified MgH_2 composites, and alloyed Mg-based systems.

Conventional processing of PCT data often compresses each isotherm into a representative plateau pressure and reports a single plateau enthalpy as a global descriptor. This practice is appropriate for near ideal flat plateaus, but it becomes ambiguous for the sloping or segmented plateaus that are common in Mg-based systems, where the apparent equilibrium pressure evolves with reaction progress. Prior studies have shown that Mg-based dehydrogenation frequently proceeds through multiple stages and mechanisms, so the thermodynamic driving force can vary along the same progress coordinate [26–33]. Dynamic reaction enthalpy is introduced here as a progress-resolved thermodynamic descriptor for dehydrogenation. It describes the apparent local enthalpy response extracted from quasi-equilibrium segments of non-ideal PCT plateaus as the reaction proceeds. Unlike the conventional reaction enthalpy of MgH_2 dehydrogenation, which is a single-valued state-function difference between specified initial and final states under fixed conditions, dynamic reaction enthalpy does not redefine the equilibrium enthalpy itself. Rather, it characterizes how the thermodynamic response is expressed along reaction progress when the measured equilibrium pressure varies with reaction progress. This treatment preserves thermodynamic consistency while revealing progress-dependent thermodynamic heterogeneity that cannot be captured by a single constant enthalpy value.

To distinguish empirical curve reconstruction from progress-resolved thermodynamic inversion, two complementary reconstruction routes are implemented and benchmarked against experimental PCT curves. Route 1 provides an empirical baseline for curve-level comparison, whereas Route 2 reconstructs PCT behavior while extracting

dynamic reaction enthalpy. The workflow first maps composition to a normalized reaction-progress coordinate and applies consistent data harmonization across temperatures to enable pointwise comparison. In PCT-based plots, reaction fraction denotes the hydrogen-content state, with 0 and 1 representing the hydrogen-free and fully hydrogenated states, respectively. In the characterization of dynamic parameters, reaction progress denotes dehydrogenation only and is normalized from 0 to 1. Route 1 determines the reference plateau reaction enthalpy (RPRE) through cross-temperature Van't Hoff regression using the equilibrium pressures at 50% reaction progress. The same criterion is applied to multi-plateau and non-ideal plateau cases within the analyzed interval to avoid subjective selection of local plateau segments. Each isotherm is then fitted as a smooth function of reaction progress using a twelfth-order polynomial, which is chosen to reproduce non-ideal PCT morphology while preserving a compact empirical baseline for direct curve-level benchmarking, and the coefficients are provided in Table S1 and Table S2. Route 2 reconstructs PCT behavior through progress-resolved thermodynamic inversion and simultaneously yields the dynamic reaction enthalpy evolution. A set of representative progress points is defined within the analysis window. For each temperature, equilibrium pressures corresponding to these fixed progress points are extracted from the isotherm so that pointwise correspondence is enforced across temperatures. At each progress point, a dedicated cross-temperature regression is then performed to infer the local thermodynamic quantities, and repeating this procedure across all progress points produces a continuous dynamic reaction enthalpy trajectory along reaction progress. The resulting trajectory is further averaged over reaction progress to obtain the global average reaction enthalpy (GARE). The inverted progress-resolved parameters are finally used to reconstruct isotherms and are compared with experimental PCT curves, which provides an internal consistency check and a direct test of practical usability. The reconstructed outputs from both routes are finally compared with experimental PCT curves, which provides a common validation basis for reconstruction quality. A schematic of the overall workflow is provided in Fig. 1. Detailed derivations and step-by-step operational procedures are given in Supporting Information, Section S1.

3. Results and discussion

3.1. Dual-path reconstruction benchmarked against PCT curves

To benchmark the practical fidelity of the dual-path reconstruction strategy under non-ideal PCT behavior, representative Mg-based systems were analyzed by comparing the two reconstruction routes against experimental PCT curves. Six systems were considered, including MgH_2 (low-T), MgH_2 (high-T), MgH_2-Al, MgH_2-NiVN, Mg—Ni, and Mg-Ni-TiS_2 [34–38]. The datasets were collected from literature-reported PCT curves, as shown in Fig. 2. These representative systems span pure MgH_2 with high and low temperature dehydrogenation regimes, MgH_2 modified by single component or multi-component catalysts, and Mg-based hydrides derived from binary or multi-component alloying. For direct comparison, Fig. 2(a1-f1) shows the polynomial reconstructions together with the corresponding experimental PCT curves, whereas Fig. 2(a2-f2) shows the reconstructed PCT curves obtained by substituting stage-specific dynamic reaction enthalpy into the Van't Hoff relation for the same datasets. Both methods reproduce plateau segments reasonably well, whereas polynomial reconstruction more readily accumulates deviations at the onset and tail regions, particularly for non-ideal isotherms with sloping or segmented plateaus and pronounced endpoint upturns. In contrast, the reconstruction obtained by introducing stage-specific dynamic reaction enthalpy into the Van't Hoff relation adapts the thermodynamic response along reaction progress and therefore better preserves curvature and transition details in complex PCT morphology, whereas the difference becomes less evident for

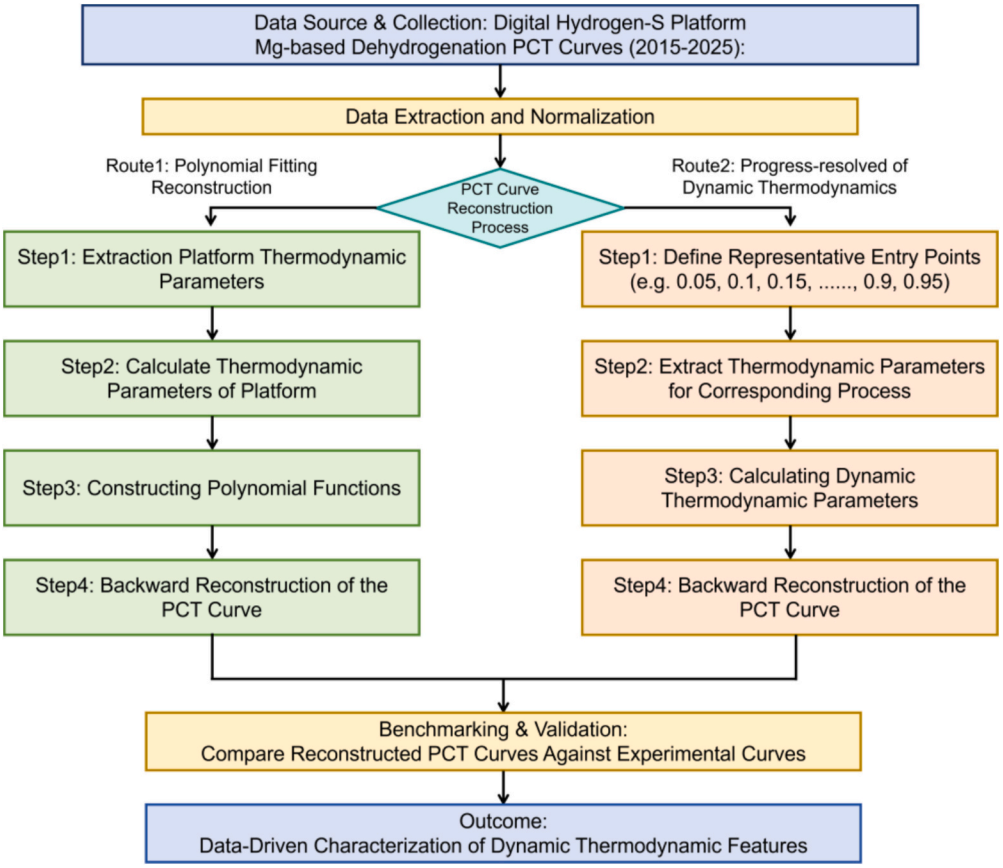

Fig. 1. Schematic diagram of dynamic thermodynamic reconstruction and polynomial fitting process for PCT curves.

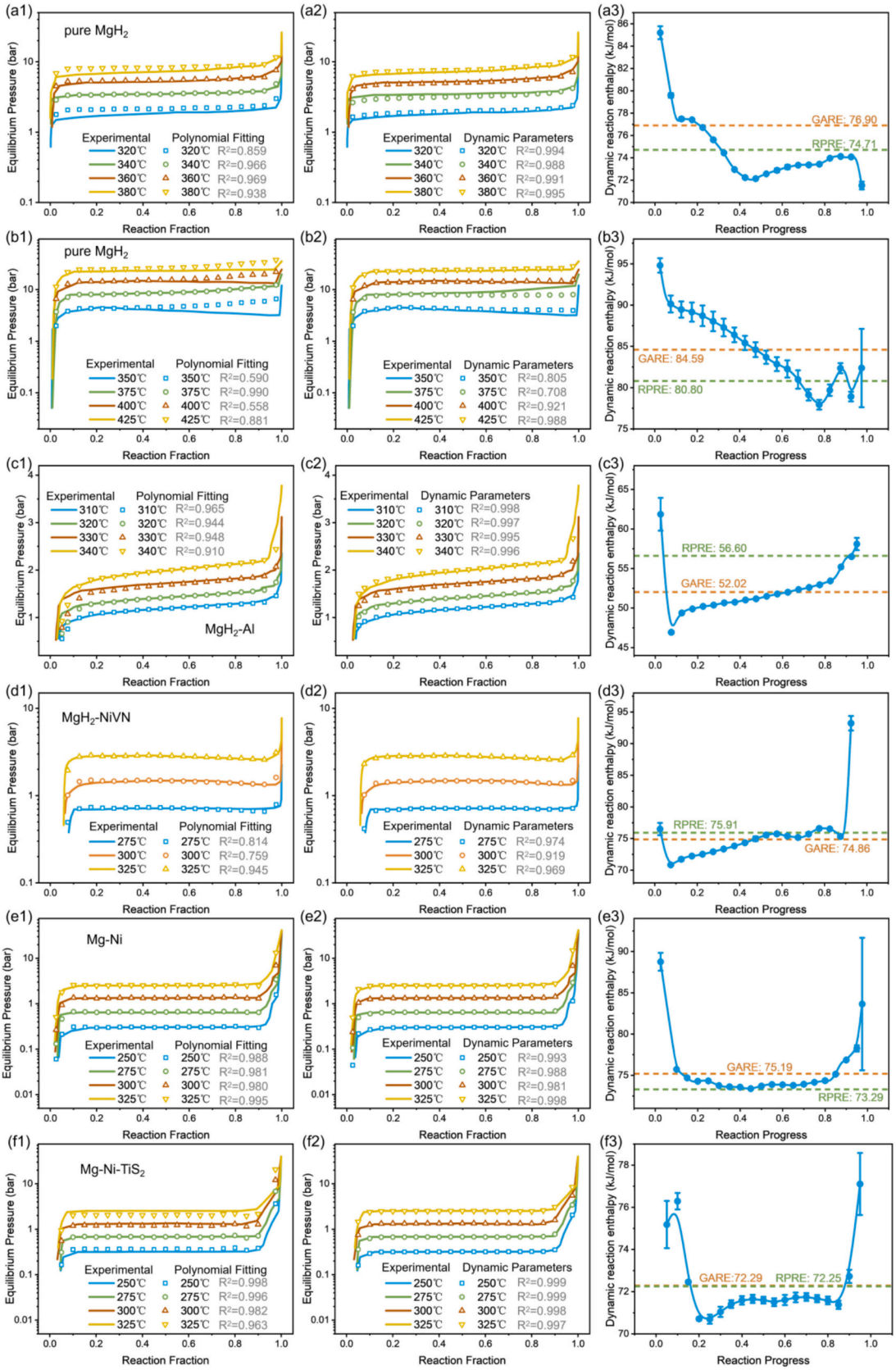

Fig. 2. Literature-reported experimental PCT curves of representative Mg-based hydrogen storage materials with two reconstruction routes [34–38]. (a1-f1) Polynomial reconstructions together with the corresponding experimental PCT curves. (a2-f2) Fitted reconstruction results obtained by inverting dynamic thermodynamic parameters. (a3-f3) Evolution of dynamic reaction enthalpy with reaction progress (GARE and RPRE represent the global average reaction enthalpy and the reference plateau reaction enthalpy, respectively).

relatively flat plateaus with mild variations.

The polynomial route provides a convenient phenomenological baseline for PCT curve reconstruction, offering a compact mathematical representation of curve morphology. However, because the fitted polynomial coefficients do not have a unique physical mapping to progress-resolved thermodynamic states, this route is not intended to deliver mechanistic thermodynamic descriptors. By contrast, introducing dynamic reaction enthalpy into the Van't Hoff relation makes the reconstructed PCT behavior thermodynamically interpretable on a progress-resolved basis, thereby linking variations in curve morphology to the evolution of thermodynamic response along reaction progress. Fig. 2(a3-f3) reports the extracted evolution of dynamic reaction enthalpy along reaction progress, which provides the progress-dependent thermodynamic input required by Route 2 and further indicates that a single constant descriptor may be insufficient to represent the full process, consistent with prior discussions of staged behavior in Mg-based dehydrogenation [17]. Notably, the close agreement between GARE and RPRE across the representative systems shows that, although dynamic reaction enthalpy varies with reaction progress, its overall average remains close to the conventional single-value enthalpy estimate. This supports the physical significance of the inverted thermodynamic response rather than suggesting a purely mathematical artifact. The quantitative accuracy and cross-sample comparability remain constrained by the quality of PCT data, including experimental noise, plateau slope and segmentation, sparse endpoint points, and the distribution of isotherm temperatures, all of which can propagate uncertainty in the inversion, especially for strongly non-ideal systems [19,29].

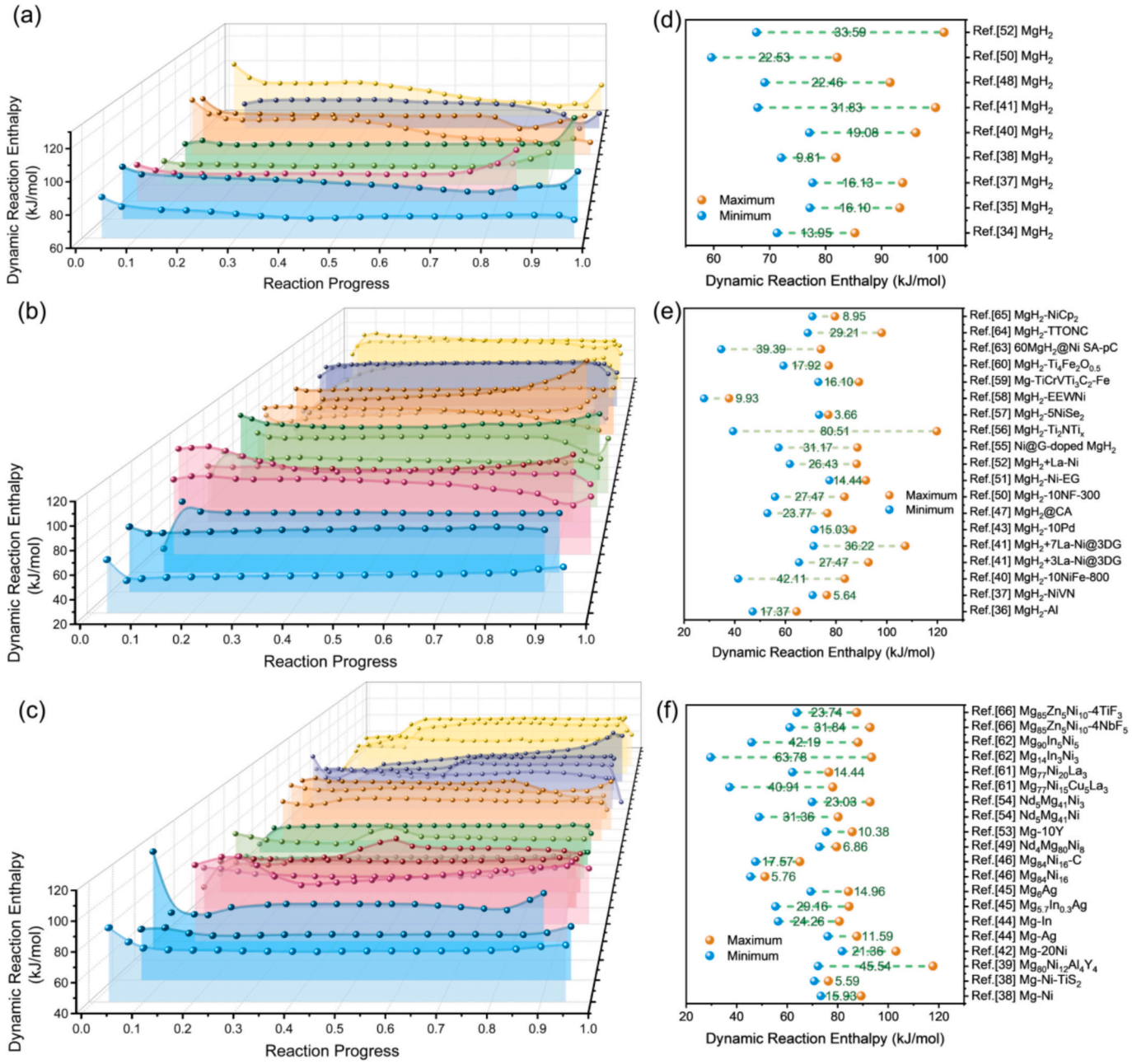

Fig. 3. The literature compilation presents the dynamic reaction enthalpy values for three categories of magnesium-based hydrogen storage materials, along with the maximum and minimum values observed in these enthalpy [34–66]. (a,d) Pure MgH_2 systems. (b,e) Catalyst-modified MgH_2 composite systems. (c,f) Mg-based alloy systems.

3.2. Compilation of dynamic reaction enthalpy data

With the reconstruction routes established, dynamic reaction enthalpy data are compiled across a broader set of Mg-based materials to extract statistical trends. All datasets are derived from literature-reported PCT curves and processed using a consistent inversion workflow. Cross-material comparability is facilitated by adopting normalized reaction progress as a unified horizontal coordinate [34–66]. To improve statistical reproducibility, only datasets containing at least three PCT isotherms and a temperature span of at least 30 K were included in the analysis. Data sources and auxiliary results are provided in the Supporting Information (Figs. S1-S47 and Table S3). Fig. 3 summarizes the compiled dynamic reaction enthalpy trajectories, and further reports the within-material ranges defined by the maximum and minimum values and their differences. For pure MgH_2, the trajectories consistently show an early-stage decrease followed by a stabilized regime. This pattern is consistent with a transition from initiation-sensitive thermodynamic responses to a plateau-constrained two-phase transformation regime [67–69]. At low reaction progress, the apparent thermodynamic response is sensitive to evolving near-surface states and the development of Mg and Mg/MgH_2 interfacial regions, yielding a rapid decline in progress-resolved dynamic reaction enthalpy. As reaction progress increases, a macroscopic two-phase coexistence region becomes established and dominates equilibrium behavior, resulting in a comparatively stable dynamic reaction enthalpy over the mid-progress regime.

For catalyst-modified MgH_2 systems, Fig. 3(b) resolves two dominant early-stage trajectory types, namely decrease-then-stabilize and increase-then-stabilize. The divergence is primarily governed by the extent and mode of catalyst-induced surface and interfacial modification, whereas the mid-progress regime remains largely constrained by two-phase plateau equilibrium. In the decrease-then-stabilize type, dynamic reaction enthalpy starts at a higher level and drops rapidly before convergence, consistent with an initiation stage controlled by evolving interfacial states followed by plateau-controlled transformation. This behavior is frequently associated with inorganic surface-activation routes, where transition-metal compounds and their in situ derived active phases accelerate interfacial reconstruction and the establishment of reactive Mg/MgH_2 boundaries, as reflected by oxide-derived and multi-metal interfacial systems in the compiled dataset. In contrast, the increase-then-stabilize type is more often observed when initiation is strongly pre-activated by interfacial electronic modulation. In such cases, the earliest apparent enthalpy response shifts to lower values and rises toward a plateau-level steady state as bulk two-phase equilibrium becomes dominant. This category includes C-based and graphene-related interfaces and Ni-based active phases coupled with heterogeneous coordination or multi-component regulation, exemplified by $60MgH_2$@Ni SA-pC [63]. These opposite early-stage trends are therefore not contradictory. Both indicate that catalysts mainly reshape the surface and interfacial environment during initiation, while the sign of the early deviation reflects whether the dominant effect is removal of interfacial limitations or strong electronic coupling that destabilizes near-surface Mg—H bonding before the plateau regime governs [70,71].

Mg-based alloy systems in Fig. 3(c) exhibit more diverse progress-dependent trajectories, reflecting more complex reaction mechanisms and phase-transformation scenarios introduced by alloying. Dual plateaus emerge in certain alloys, where the PCT curve displays two plateau regions and the corresponding dynamic reaction enthalpy trajectory shows two plateau-like intervals, as exemplified by $Mg_{5.7}In_{0.3}Ag$ and $Mg_{77}Ni_{15}Cu_5La_3$ [45,61]. This behavior indicates at least two thermodynamically distinguishable equilibrium steps separated by a transition region, consistent with a mechanism switch between plateau regimes. Beyond the trajectory shapes, Fig. 3(d-f) quantifies the span of dynamic reaction enthalpy within each material as the difference between its maximum and minimum values across reaction progress. The mean span is 20.60 kJ/mol for pure MgH_2, 24.70 kJ/mol for catalyst-modified composites, and 24.00 kJ/mol for Mg-based alloys. The broader spans and occasional extreme cases in the latter two categories are consistent with stronger progress-dependent thermodynamic heterogeneity induced by interfacial reconstruction, non-ideal plateau behavior, and multi-process participation. These statistics highlight that thermodynamic differences across reaction progress are not negligible, and that collapsing the process into a single constant enthalpy can obscure stage-specific driving-force variations that are critical for cross-system comparison and mechanism interpretation.

Terminal-stage behaviors beyond roughly 90% reaction progress vary across materials, with dynamic reaction enthalpy showing increases, enhanced fluctuations, or secondary decreases. Contributing factors include differences in PCT measurements, sample-preparation-induced heterogeneity, bed-level heat transfer and local non-equilibrium effects, and amplified inversion uncertainty due to sparse endpoint data, which together compromise late-stage cross-material comparability [72]. The terminal rebound or strongly fluctuating region is therefore not aggregated. The analysis focuses on cross-material consistent regimes, including the early dynamic state and the plateau-stabilized regime [73,74]. Overall, this compilation extends conventional single-value plateau descriptions to a progress-resolved dynamic reaction enthalpy spectrum and provides a stage-structured thermodynamic signature for Mg-based dehydrogenation at a statistical scale. It also establishes a physically interpretable reference for subsequent thermodynamic-kinetic coupling analyses.

3.3. The significance of dynamic thermodynamics for engineering applications

To characterize the system-dependent dispersion between globally averaged thermodynamic descriptors and literature reporting and to assess its engineering implications, the deviation between GARE and RPRE was systematically analyzed for three categories of Mg-based systems, as shown in Fig. 4. The differences defined as GARE minus RPRE span from −3.05 to +4.03 kJ/mol for pure MgH_2, from −5.20 to +15.29 kJ/mol for catalyst-modified composites, and from −16.52 to +10.80 kJ/mol for Mg-based alloys, while the corresponding absolute mean differences are 2.24, 4.19, and 4.62 kJ/mol, respectively. Pure MgH_2 shows a narrow distribution centered near zero, whereas catalyst-modified composites and Mg-based alloys exhibit substantially broader dispersion, indicating that globally averaged enthalpy remains more consistent with literature-reported values under relatively simple plateau behavior than under non-ideal or multistage transformations. In catalyst-modified systems, the broader spread is mainly associated with catalyst-dependent changes in plateau shape and hysteresis, together with differences in quasi-equilibrium assessment during PCT acquisition and thermodynamic extraction. In Mg-based alloys, multiphase coexistence, compositional redistribution, and multi-plateau behavior further complicate the definition of an equivalent thermodynamic descriptor, so a single reported enthalpy may reflect only a segment-specific transformation step rather than the full reaction process.

From an engineering perspective, the deviation is not only a validation metric but also a practical indicator of thermodynamic uncertainty that can propagate through the entire chain from materials screening to reactor design and operation. Thermodynamic inputs directly determine heat-duty estimation, heating power sizing, and heat-exchanger capacity allocation, and systematic underestimation or overestimation can translate into inefficient energy budgeting, delayed hydrogen-release response, or temperature overshoot during high-rate and transient operation. The broad dispersion observed in complex systems underscores that progress-dependent thermodynamic differences are non-negligible and that relying on a single literature value can mask stage-specific heat demand and driving-force variations, which are critical under fluctuating load and limited thermal headroom. Quantifying this deviation therefore enables uncertainty-bounded parameter selection for engineering models, supports robust design margins and

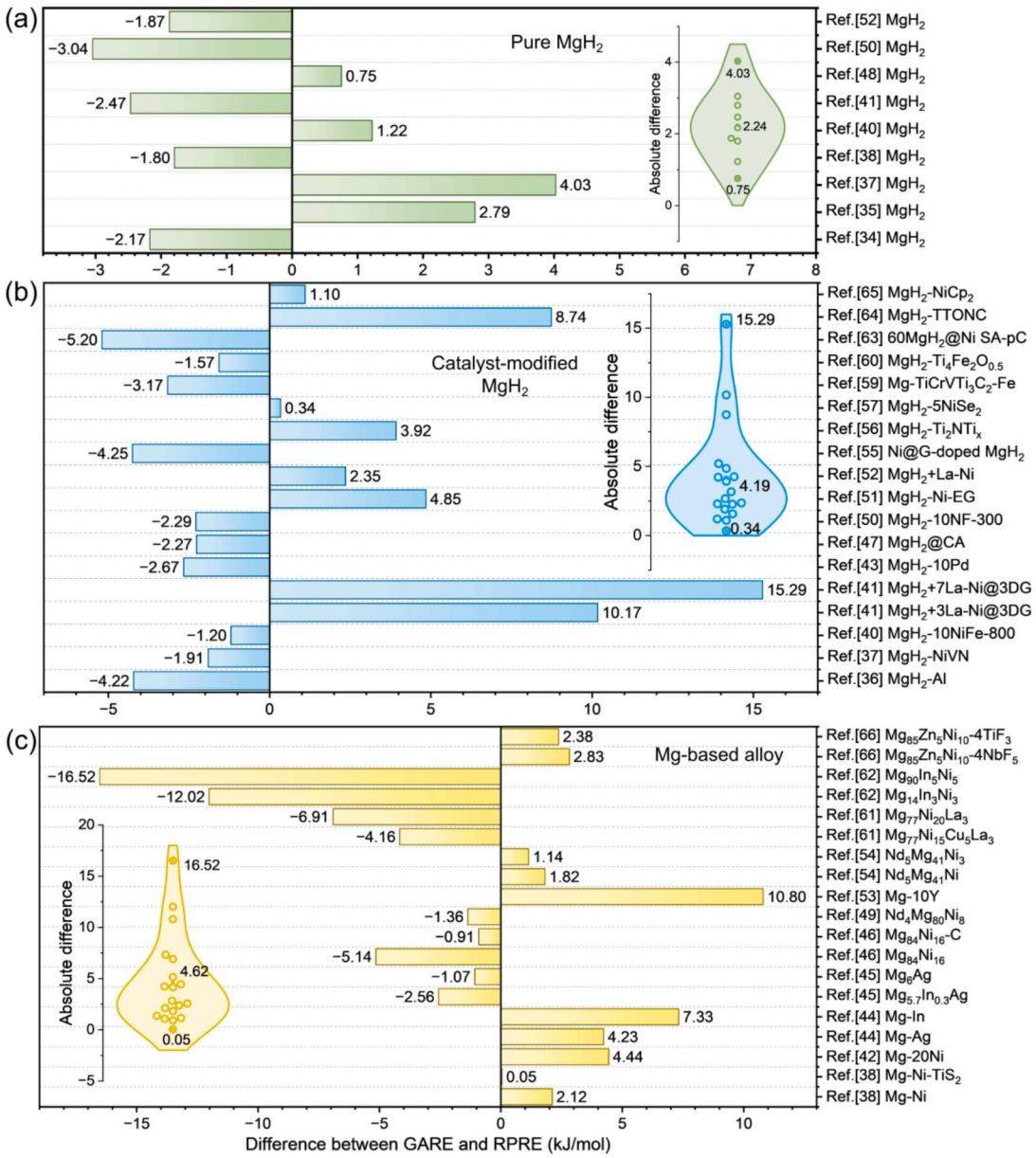

Fig. 4. Statistical analysis of the difference between GARE and RPRE in three types of magnesium-based hydrogen storage material systems [34–66]. (a) Pure MgH_2 systems. (b) Catalyst-modified MgH_2 composite systems. (c) Mg-based alloy systems.

risk-aware operation envelopes, and motivates stage-aware heat-demand budgeting based on progress-resolved dynamic reaction enthalpy. In this sense, the deviation analysis provides a bridge between thermodynamic data quality and engineering reliability, and offers a data-grounded route to translate non-ideal PCT information into more resilient thermal design, control-oriented operation, and system-level performance prediction for Mg-based solid-state hydrogen storage modules.

3.4. Progress-resolved coupling between dynamic reaction enthalpy and apparent activation energy

Thermodynamic and kinetic descriptors may exhibit parallel evolution along reaction progress. On this basis, we examine whether dynamic reaction enthalpy and apparent activation energy show repeatable co-variation patterns along reaction progress. This comparison enables a progress-resolved discussion of dynamic reaction enthalpy in parallel with dynamic apparent activation energy. It should be emphasized that both quantities in this work are obtained through numerical inversion and fitting of PCT-derived information, and their absolute values inevitably contain systematic bias and inversion uncertainty arising from experimental noise, model assumptions, and data sparsity. Accordingly, this section does not aim to establish a strict one-to-one numerical correspondence, a mechanistic causal relationship, or a quantitatively calibrated linear relationship between thermodynamic and kinetic parameters. Instead, the analysis focuses on stage-resolved features along reaction progress, including relative trend consistency, turning-point correspondence, and the repeatability of these coupled evolution characteristics across different material classes. Following this progress-resolved perspective, Fig. 5 presents the evolution of dynamic reaction enthalpy, the evolution of dynamic apparent activation energy, and their trend correspondence on a unified reaction progress axis for pure MgH_2, catalyst-modified MgH_2, and Mg-based alloy systems.

Across these materials, progress-resolved dynamic reaction enthalpy and dynamic apparent activation energy co-evolve, with broadly aligned turning positions separating an early rapidly varying regime from a mid-progress stabilized regime. For pure MgH_2, the coupling manifests as

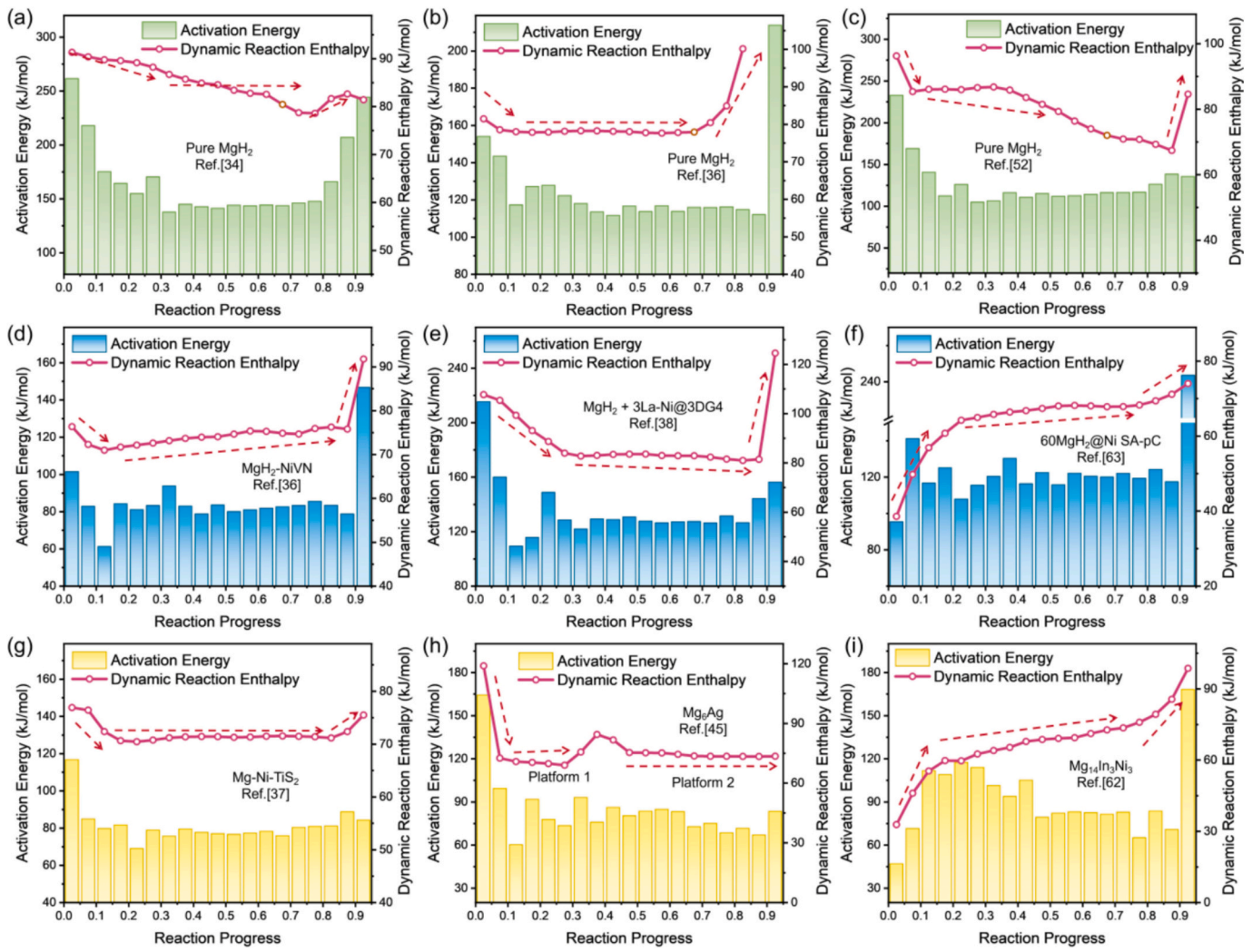

Fig. 5. Progress-resolved coupling between dynamic reaction enthalpy and apparent activation energy in representative Mg-based dehydrogenation systems [34,36–38,45,52,62,63]. (a-c) pure MgH_2, (d-f) catalyst-modified MgH_2 composites, and (g-i) Mg-based alloy systems.

synchronous adjustment at initiation followed by co-stabilization within the plateau-dominated regime [34,36,52]. This behavior is attributable to concurrent evolution of the local Mg—H bonding environment and the interfacial chemical-potential landscape at the Mg/MgH_2 front, which jointly reshapes the effective enthalpy scale and the barrier scale of the rate-controlling step. Once the two-phase plateau is established, both descriptors become constrained and tend to converge. For catalyst-modified systems, Fig. 5(d,e) show NiVN and $NiSe_2$ exhibiting a decrease-then-stabilize trajectory, where both curves turn and stabilize within the same progress window [36,38]. This alignment suggests that catalysts primarily act through surface and interfacial modification during initiation, tuning the local Mg—H bond-breaking environment and interfacial reconstruction barrier in concert before plateau constraints dominate. Catalyst-derived active interfaces and defect-rich contact regions can further modify near-surface hydrogen chemical potential and local driving force, promoting coordinated evolution of thermodynamic response and kinetic threshold. Fig. 5(f) illustrates an increase-then-stabilize pattern, consistent with stronger interfacial coupling or more pronounced Mg—H weakening that elevates both thermodynamic and barrier scales at initiation, while convergence still occurs once plateau-governed two-phase transformation dominates [63]. For Mg-based alloys, Fig. 5(g-i) also shows enthalpy-barrier coupling, but the detailed shapes depend on multiphase participation and complex phase-transition pathways [37,45,62]. Alloying introduces distinct hydrogen configurations and bonding motifs, and secondary phases impose additional equilibrium constraints, such that different progress windows can correspond to different rate-controlling steps and effective reaction coordinates. Dual-plateau alloys exemplify this behavior, where segmented coupling and a coupled stage transition emerge across two plateau-related progress windows, consistent with at least two thermodynamically distinguishable equilibrium steps separated by a transition regime.

3.5. *Mechanistic origin of the progress-dependent thermodynamics and kinetics co-evolution*

Thermodynamic-kinetic co-evolution refers to the correspondence between the turning points and stagewise stabilization of dynamic reaction enthalpy and apparent activation energy during dehydrogenation. This behavior arises from the migration of the rate-controlling step and from the continuous reconstruction of interfaces and the reaction front [75–77]. Fig. 6 presents an atomic-scale schematic of this progress-resolved framework for MgH_2 and catalyzed MgH_2. It maps surface dehydrogenation to defect-rich surface regions, phase transition nucleation and interface advance to the bulk transformation zone, and terminal islanding to spatially isolated residual MgH_2 domains embedded in the Mg-rich product. Alloy systems are not discussed here because multiphase coexistence, compositional redistribution, and multi-plateau

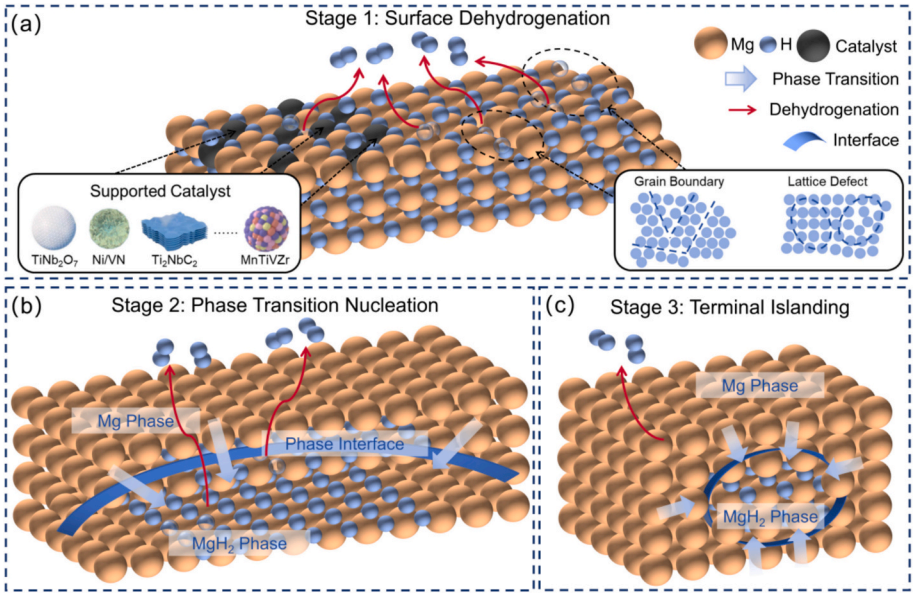

Fig. 6. Spatially resolved schematic of stage dependent dehydrogenation mechanisms in MgH_2. (a) Surface dehydrogenation, (b) Phase transition nucleation and (c) Terminal islanding.

transformations can superimpose multiple subprocesses on the same progress coordinate, thereby compromising mechanistic identifiability. When an alloy exhibits a single plateau, or a clearly segmentable plateau feature within a defined temperature and pressure window, and when distinct transformation intervals can be separated along reaction progress, the logic developed here remains applicable on a plateau-by-plateau basis. On this basis, the following discussion analyzes the mechanism along reaction progress and links interface evolution to the coupled trends of dynamic reaction enthalpy and apparent activation energy.

3.5.1. Stage 1. Energy landscape reconstruction triggered by interfacial initiation and reaction front propagation (surface dehydrogenation)

Dehydrogenation initiates preferentially at interfaces such as surfaces, grain boundaries, and defect-rich regions [78–80]. As the reaction front advances into the particle interior, the local coordination environment, defect density, and interfacial chemical state evolve rapidly, reshaping the effective reaction pathway and the transition-state landscape. Experimental evidence has captured nucleation-and-growth features during MgH_2 dehydrogenation together with outside-to-inside propagation of the transforming region, supporting interface-governed initiation and rapid early-stage energy-landscape rearrangement [81]. In this window, dynamic reaction enthalpy is more sensitive to interfacial heterogeneity and therefore shows a pronounced adjustment. Apparent activation energy can also vary in a stage-dependent manner because bond-breaking and mass-transport barriers are redistributed. In catalyzed MgH_2, the catalyst modifies the interfacial chemical state and local reaction pathway, which facilitates this rearrangement and strengthens the coupled turning behavior at the beginning of dehydrogenation [82–84].

3.5.2. Stage 2. Quasi steady locking dominated by the phase transformation plateau (phase transition nucleation)

After entering the two-phase coexistence regime associated with the pressure plateau, transformation proceeds primarily via sustained motion of phase boundaries within a relatively narrow chemical-potential window. The dominant pathway type and phase-boundary evolution statistics become more stable, establishing a quasi steady progression [85,86]. Accordingly, dynamic reaction enthalpy remains relatively flat over a finite progress interval, and the fluctuation amplitude of apparent activation energy decreases, reflecting plateau-driven locking of the coupled trend. Kinetic modeling under constant pressure indicates that when the thermodynamic driving force is approximately stable within the plateau regime, the reaction rate exhibits a more stable stage-wise behavior, consistent with quasi steady locking [87]. Catalysis can shift the onset, termination, and stability of the locking interval, while the plateau regime remains governed by phase-boundary propagation [88–92].

3.5.3. Stage 3. Hindrance enhancement induced by terminal depletion and interface recession (terminal islanding)

At high reaction progress, the active phase is gradually depleted, the reaction front contracts, and the effective phase-boundary area decreases, reducing the number of reactive sites. As the interface recedes, the remaining MgH_2 can become spatially isolated as residual domains embedded in the Mg-rich matrix, so dehydrogenation proceeds within confined islands rather than along an extended front. Thickening product layers and elongated diffusion pathways intensify mass-transfer limitations, increasing kinetic hindrance and manifesting as an upturn or enlarged fluctuations in apparent activation energy [93]. Prior studies have shown that hydrogen uptake and release in magnesium-based systems can become controlled by solid-state hydrogen diffusion in certain regimes, rationalizing diffusion-limited rate decay that is more readily expressed near the end of dehydrogenation [94–97]. In parallel, dynamic reaction enthalpy is more likely to deviate from plateau-like flat behavior and can show a rebound or increased dispersion. For catalyzed MgH_2, an additional decrease in effective catalytic interface can further amplify the terminal deviation.

The terminal anomalies should be distinguished between mechanistic effects and the stability boundary of inversion. At high reaction progress, the signal-to-noise ratio decreases and heat and mass transfer constraints become stronger, so dynamic reaction enthalpy and apparent activation energy are more susceptible to sparse end-point data, amplified interpolation or fitting errors, measurement noise, and local non-equilibrium effects [29]. Reactor-scale experiments and simulations further indicate that coupled heat and mass transfer constraints can substantially affect apparent kinetics and performance in the late stage of MgH_2 dehydrogenation, increasing the likelihood of non-intrinsic deviations in the terminal regime [98–100]. Therefore, terminal behavior should be interpreted on the basis of interval-level

consistency rather than single-point excursions, and the credible range of the inverted results should be constrained by uncertainty evaluation in subsequent analysis.

4. Conclusions

This study addresses the challenge of progress-resolved thermodynamic characterization during dehydrogenation of Mg-based solid-state hydrogen storage materials. A data-driven analytical framework is developed based on pressure-composition-temperature curves to extract dynamic reaction enthalpy along reaction progress and to benchmark its evolution across pure MgH_2, catalyst-modified composites, and Mg-based alloys. The framework is validated by PCT back-reconstruction and shows improved fidelity over a polynomial regression baseline in preserving non-ideal plateau morphology and progress-dependent turning behavior. Literature-scale analyses further confirm non-negligible within-material enthalpy spans and pronounced system-dependent differences between globally averaged enthalpy and literature-reported values. Thermodynamic-kinetic coupling analyses further demonstrate repeatable co-variation between dynamic reaction enthalpy and dynamic apparent activation energy with aligned turning positions. These observations support coupled thermodynamic-kinetic evolution and are organized into a stage-structured, three-mechanism framework spanning interface establishment, plateau-governed two-phase transformation, and late-stage depletion with strengthened mass-transfer limitation.

Overall, this work renders thermodynamic information embedded in pressure-composition-temperature data computable and comparable in a progress-resolved manner. It provides a general methodological basis for quantitative mechanism interrogation of Mg-based solid-state hydrogen storage materials and supplies a stage-aware heat-demand descriptor to support heat-duty estimation, thermal design, and robust transient operation of practical dehydrogenation reactors. Future work should expand the material spectrum under stricter data-quality control to build a standardized progress-resolved thermodynamic database. Integrating this framework with multiphysics modeling, data assimilation, and machine learning will further enable a closed loop from curve inversion to mechanism recognition, parameter mapping, and performance prediction, thereby supporting material design and dynamic control strategies under engineering-relevant operating conditions.

CRediT authorship contribution statement

Jianghao Cai: Writing – review & editing, Writing – original draft, Visualization, Software, Methodology, Formal analysis, Data curation. **Yutian Zhuang:** Visualization, Formal analysis. **Kang Ma:** Formal analysis, Data curation. **Yutong Jiang:** Formal analysis, Data curation. **Xuao Lu:** Visualization, Methodology. **Zhengyang Gao:** Writing – review & editing, Methodology, Funding acquisition. **Weijie Yang:** Writing – review & editing, Visualization, Supervision, Funding acquisition, Conceptualization.

Declaration of Generative AI and AI-assisted technologies in the writing process

During the preparation of this work, the authors used ChatGPT in order to improve language expression and check grammar. After using this tool, the authors reviewed and edited the content as needed and take full responsibility for the content of the publication.

Declaration of competing interest

The authors declare that they have no known competing financial interests or personal relationships that could have appeared to influence the work reported in this paper.

Acknowledgements

This work was supported by Beijing Natural Science Foundation (2262076), Natural Science Foundation of Hebei Province (E2025502039), Fundamental Research Funds for the Central Universities (2025JC008 and 2025MS131).

Appendix A. Supplementary data

Supplementary data to this article can be found online at https://doi.org/10.1016/j.est.2026.122655.

Data availability

Data will be made available on request.

References

[1] Q. Zhang, Y. Shan, J. Pan, et al., A photovoltaic-electrolysis system with high solar-to-hydrogen efficiency under practical current densities, Science Advances 11 (2025) eads0836.
[2] S. Zhou, W. Cao, L. Shang, et al., Facilitating alkaline hydrogen evolution kinetics via interfacial modulation of hydrogen-bond networks by porous amine cages, Nat. Commun. 16 (2025) 1849.
[3] X. Zhang, S. Ju, C. Li, et al., Atomic reconstruction for realizing stable solar-driven reversible hydrogen storage of magnesium hydride, Nat. Commun. 15 (2024) 2815.
[4] H. Yang, Z. Ding, Y. Li, et al., Recent advances in kinetic and thermodynamic regulation of magnesium hydride for hydrogen storage, Rare Metals 42 (9) (2023) 2906–2927.
[5] W. Fu, Y. Li, Z. Dong, et al., Digital hydrogen-S: an open-access interactive data platform for solid-state hydrogen storage materials, Int. J. Hydrogen Energy 207 (2026) 153434.
[6] Z. Ding, Y. Li, H. Yang, et al., Tailoring MgH_2 for hydrogen storage through nanoengineering and catalysis, J. Magnesium Alloys 10 (2022) 2946–2967.
[7] L. Zhang, F. Nyahuma, H. Zhang, et al., Metal organic framework supported niobium pentoxide nanoparticles with exceptional catalytic effect on hydrogen storage behavior of MgH_2, Green Energy & Environment 8 (2023) 589–600.
[8] W. Shi, F. Hong, R. Li, et al., Improved hydrogen storage properties of MgH_2 by Mxene (Ti_3C_2) supported MnO_2, J. Energy Storage 72 (2023) 108738.
[9] M. Song, F. Wu, Y. Jiang, et al., Optimizing FeCoNiCrTi high-entropy alloy with hydrogen pumping effect to boost de/hydrogenation performance of magnesium hydride, Rare Metals. 43 (7) (2024) 3273–3285.
[10] S. Li, L. Zhang, F. Wu, et al., Efficient catalysis of FeNiCu-based multi-site alloys on magnesium-hydride for solid-state hydrogen storage, Chin. Chem. Lett. 36 (2025) 109566.
[11] Z. Zheng, C. Peng, Q. Zhang, Structural features of 18R-type long-period stacking ordered phase in $Mg_{85}Zn_6Y_9$ alloy and the Ni doping effect on its hydrogen storage properties, J. Mater. Sci. Technol. 145 (2023) 148–155.
[12] N.S. Norberg, T.S. Arthur, S.J. Fredrick, et al., Size-dependent hydrogen storage properties of Mg nanocrystals prepared from solution, J. Am. Chem. Soc. 133 (2011) 10679–10681.
[13] H. Kim, H. Kim, W. KimFacile, et al., Synthesis of nanoporous Mg crystalline structure by organic solventbased reduction for solid-state hydrogen storage, Nat. Commun. 15 (2024) 10800.
[14] J. Karst, F. Sterl, H. Linnenbank, et al., Watching in situ the hydrogen diffusion dynamics in magnesium on the nanoscale, Sci. Adv. 6 (2020) eaaz0566.
[15] X. Tang, J. Cai, T. Yao, et al., Revealing the role of grain boundaries in magnesium-based hydrogen storage: insights into adsorption and dissociation, J. Mater. Chem. A 13 (2025) 38252–38261.
[16] H. Yun, H. Wang, J. Bai, et al., Activation and hydrogen storage properties of Mg-based composites synthesized by catalytic mechanochemical hydrogenation strategy, Int. J. Hydrogen Energy 50 (2024) 1025–1039.
[17] S. Dong, C. Li, J. Wang, et al., The "burst effect" of hydrogen desorption in MgH_2 dehydrogenation, J. Mater. Chem. A 10 (2022) 22363–22372.
[18] C. Li, W. Yang, H. Liu, et al., Picturing the gap between the performance and US-DOE's hydrogen storage target: a data-driven model for MgH_2 dehydrogenation, Angew. Chem. Int. Ed. 63 (28) (2024) e202320151.
[19] J. Cai, H. Wang, X. Tang, et al., Data-driven evidence for the burst effect in MgH_2 dehydrogenation via analysis of experimental kinetic curves, J. Energy Storage 136 (2025) 118450.
[20] J. Cai, Y. Jiang, T. Yao, et al., A demand-driven dynamic heating strategy for ultrafast and energy-efficient MgH_2 dehydrogenation utilizing the "burst effect", J. Energy Storage 130 (2025) 117495.
[21] V.K. Sharma, E.A. Kumar, S.S. Murthy, Influence of dynamic operating conditions on the performance of metal hydride based solid sorption cooling systems, Int. J. Hydrogen Energy 40 (2015) 1108–1115.
[22] M. Kandavel, S. Ramaprabhu, Hydriding properties of Ti-substituted non-stoichiometric AB_2 alloys, J. Alloys Compd. 381 (2024) 140–150.

[23] A. Jai, R.K. Jain, S. Agarwal, et al., Structural and thermodynamical investigations of $La_{0.23}Ni_{0.34}Co_{0.33}Nd_{0.08}Ti_{0.01}Al_{0.01}$ hydrogen storage alloy, Int. J. Hydrogen Energy 33 (2008) 356–359.
[24] H. Su, X. Ma, K. Sun, Single-atom metal tuned sulfur vacancy for efficient H_2 activation and hydrogen evolution reaction on MoS_2 basal plane, Appl. Surf. Sci. 597 (2024) 153614.
[25] T.T. Yang, W.A. Saidi, The Bell-Evans-Polanyi relation for hydrogen evolution reaction from first-principles, npj Comput. Mater. 10 (2024) 98.
[26] L. Ren, Y. Li, N. Zhang, et al., Nanostructuring of Mg-based hydrogen storage materials: recent advances for promoting key applications, Nano-Micro Lett. 15 (2023) 93.
[27] H. Jiang, Z. Ding, Y. Li, et al., Hierarchical interface engineering for advanced magnesium-based hydrogen storage: synergistic effects of structural design and compositional modification, Chem. Sci. 16 (2025) 7610.
[28] H. Wang, J. Li, X. Wei, et al., Thermodynamic and kinetic regulation for Mg-based hydrogen storage materials: challenges, strategies, and perspectives, Adv. Funct. Mater. 34 (42) (2024) 2406639.
[29] F. Yang, Y. Zhang, F. Ciucci, et al., Towards a consistent understanding of the metal hydride reaction kinetics: measurement, modeling and data processing, J. Alloys Compd. 741 (2018) 610–621.
[30] Q. Li, X. Lin, Q. Luo, et al., Kinetics of the hydrogen absorption and desorption processes of hydrogen storage alloys: a review, Int. J. Miner. Metall. Mater. 29 (2025) 32.
[31] C. Liu, Z. Yuan, X. Li, et al., Hydrogen storage capabilities enhancement of MgH_2 nanocrystals, Int. J. Hydrogen Energy 88 (2024) 515–527.
[32] P. Yao, Y. Jiang, Y. Liu, et al., Catalytic effect of Ni@rGO on the hydrogen storage properties of MgH_2, J. Magnesium Alloys 8 (2020) 451–471.
[33] X. Lu, S. Luo, J. Li, et al., FIND: a forward-inverse navigation and discovery platform for hydrogen storage alloys powered by data-driven machine learning, J. Mater. Inform. 5 (2025) 48.
[34] Y. Jiang, Y. Liu, M. Yue, et al., Pulsed electrodeposited rare earth medium-entropy amorphous alloys for catalyzing MgH_2 for solid-state hydrogen storage, J. Energy Storage 107 (2025) 114956.
[35] S. Zhao, T. Wu, K. Wang, et al., Synergistic dual-modification regulation of dehydrogenation kinetics of MgH_2 by MOF-derived Core-shell Ni&C, Int. J. Hydrogen Energy 127 (2025) 241–251.
[36] H. Chen, N. Ma, C. Cheng, et al., Hydrogen activation on aluminium-doped magnesium hydride surface for methanation of carbon dioxide, Appl. Surf. Sci. 515 (2020) 146038.
[37] J. Wu, Z. Liu, H. Zhang, et al., Hydrogen storage performance of MgH_2 under catalysis by highly dispersed nickel-nanoparticle-doped hollow spherical vanadium nitride, J. Magnesium Alloys 12 (2024) 5132–5143.
[38] D. Tan, C. Peng, Q. Zhang, Microstructural characteristics and hydrogen storage properties of the Mg-Ni-TiS_2 nanocomposite prepared by a solution-based method, Int. J. Hydrogen Energy 48 (2023) 16756–16768.
[39] X. Dong, Y. Li, Y. Zhai, et al., Study on microstructure and hydrogen storage properties of $Mg_{80}Ni_{16-x}Al_xY_4$ (x = 2, 4, 8) alloys, Metals 14 (2024) 126.
[40] Y. Chen, B. Sun, G. Zhang, et al., MOF-derived $Ni_3Fe/Ni/NiFe_2O_4$@C for enhanced hydrogen storage performance of MgH_2, J. Energy Chem. 101 (2025) 333–344.
[41] J. Zhang, C. Zheng, Y. Wang, et al., Effect of La-Ni@3DG catalyst concentration on the hydrogen storage properties of MgH_2, Int. J. Hydrogen Energy 95 (2024) 666–677.
[42] J. Qiu, Y. Yang, H. Wan, et al., Interface-engineered TiV bimetal catalysts with synergistic effects for enhancing hydrogen storage performance in Mg-Ni-based material, J. Phys. Chem. Lett. 16 (2025) 8084–8091.
[43] N. Xu, H. Zhou, M. Zhang, et al., Synergistic effect of Pd single atoms and clusters on the de/re-hydrogenation performance of MgH_2, J. Mater. Sci. Technol. 191 (2024) 49–62.
[44] J. Mao, T. Huang, S. Panda, et al., Direct observations of diffusion controlled microstructure transition in Mg-In/Mg-Ag ultrafine particles with enhanced hydrogen storage and hydrolysis properties, Chem. Eng. J. 418 (2021) 129301.
[45] T. Si, Y. Cao, Q. Zhang, et al., Enhanced hydrogen storage properties of a Mg-Ag alloy with solid dissolution of indium: a comparative study, J. Mater. Chem. A 3 (2015) 8581.
[46] D. Rahmalina, R. Rahman, A. Suwandi, et al., The recent development on MgH_2 system by 16 wt% nickel addition and particle size reduction through ball milling: a noticeable hydrogen capacity up to 5 wt% at low temperature and pressure, Int. J. Hydrogen Energy 45 (2020) 29046–29058.
[47] D. Peng, Z. Ding, L. Zhang, et al., Remarkable hydrogen storage properties and mechanisms of the shellecore MgH_2@carbon aerogel microspheres, Int. J. Hydrogen Energy 43 (7) (2018) 3731–3740.
[48] X. Duan, G. Li, W. Zhang, et al., Ti_3AlCN MAX for tailoring MgH_2 hydrogen storage material: from performance to mechanism, Rare Met. 42 (6) (2023) 1923–1934.
[49] Q. Luo, Q. Gu, J. Zhang, et al., Phase equilibria, crystal structure and hydriding/dehydriding mechanism of Nd4Mg80Ni8 compound, Sci. Rep. 5 (2015) 15385.
[50] Y. Chen, X. Li, B. Sun, et al., Effect of NiFe-LDH/FeO(OH) derivatives on the hydrogen storage properties of MgH_2, Int. J. Hydrogen Energy 121 (2025) 326–336.
[51] S. Shen, L. Ouyang, J. Liu, et al., In situ formed ultrafine metallic Ni from nickel (II) acetylacetonate precursor to realize an exceptional hydrogen storage performance of MgH_2-Ni-EG nanocomposite, J. Magnesium Alloys 11 (2023) 3174–3185.
[52] C. Zheng, D. Zhou, Y. Niu, et al., Catalytic modification of MgH_2 hydrogen storage properties by La-Ni catalysts, Int. J. Hydrogen Energy 89 (2024) 760–771.
[53] Y. Guo, J. Bai, Z. He, et al., Y and Ni microalloying on Mg/MgH_2 for enhancing the hydrogenation and dehydrogenation performance, Int. J. Hydrogen Energy 141 (2025) 709–720.
[54] C. Liu, Z. Yuan, X. Li, et al., Effect of Ni content on hydrogen storage properties of Nd_5Mg_{41} alloy, J. Energy Storage 82 (2024) 110608.
[55] X. Ding, H. Ding, Y. Song, et al., Activity-tuning of supported co-Ni nanocatalysts via composition and morphology for hydrogen storage in MgH2, Front. Chem. 7 (2020) 937.
[56] L. Qin, G. Zhang, T. Liang, et al., Oxygen vacancy-rich Ti_2NTi_x MXene as a high-efficiency catalyst for enhanced hydrogen desorption of MgH_2, J. Alloys Compd. 1030 (2025) 180702.
[57] X. Ou, J. Li, H. Lv, et al., Effect of nanosized nickel diselenide on hydrogen storage properties of ball-milled magnesium hydride, Int. J. Hydrogen Energy 101 (2025) 594–604.
[58] V.N. Kudiiarov, A. Kenzhiyev, N. Kurdyumov, et al., Superior catalytic activity of nano sized Ni produced by electrical explosion of wires towards the hydrogen storage of magnesium hydride, Int. J. Hydrogen Energy 109 (2025) 436–452.
[59] Y. Chen, Z. Li, Y. Wu, et al., Synergetic effect of Ti_3C_2-X (X = Fe, Co, Ni) on enhanced hydrogen storage performance of MgH_2-TiCrV composite, J. Alloys Compd. 976 (2024) 173274.
[60] V.V. Berezovets, R.V. Denys, I.Y. Zavaliy, et al., Effect of Ti-based nanosized additives on the hydrogen storage properties of MgH_2, Int. J. Hydrogen Energy 47 (2022) 7289–7298.
[61] Y. Lv, B. Zhang, Y. Wu, Effect of Cu substitution for Ni on microstructural evolution and hydrogen storage properties of the $Mg_{77}Ni_{20-x}Cu_xLa_3$ (x = 0, 5, 10 at%) alloys, J. Alloys Compd. 645 (2015) S423–S427.
[62] Y. Lu, H. Wang, J. Liu, et al., Reversible De/hydriding reactions between two new Mg-In-Ni compounds with improved thermodynamics and kinetics, J. Phys. Chem. C 119 (2015) 26858–26865.
[63] Y. Li, L. Ren, Y. Yao, et al., A single-atom interface engineering strategy to promote hydrogen sorption performances of magnesium hydride, Adv. Funct. Mater. 35 (2025) 2417915.
[64] F. Hong, H. Fu, W. Shi, et al., Application of nitrogen-doped graphene-supported titanium monoxide as a highly active catalytic precursor to improve the hydrogen storage properties of MgH_2, J. Alloys Compd. 960 (2023) 170727.
[65] C. Peng, Y. Li, Q. Zhang, Enhanced hydrogen desorption properties of MgH_2 by highly dispersed Ni: The role of in-situ hydrogenolysis of nickelocene in ball milling process, J. Alloys Compd. 900 (2022) 163547.
[66] Y. Yin, B. Li, Z. Yuan, et al., A comparison of TiF_3 and NbF_5 catalytic effects on hydrogen absorption and desorption kinetics of a ball-milled $Mg_{85}Zn_5Ni_{10}$ alloy, RSC Adv. 8 (2018) 34525.
[67] C. Zhou, C. Hu, Y. Li, et al., Crystallite growth characteristics of Mg during hydrogen desorption of MgH_2, Prog. Nat. Sci. Mater. Int. 30 (2020) 246–250.
[68] J. Lyu, V. Kudiiarov, A. Lider, Experimentally observed nucleation and growth behavior of Mg/MgH_2 during De/hydrogenation of MgH_2/Mg: a review, Materials 15 (22) (2022) 8004.
[69] Y. Xu, Y. Zhou, Y. Li, et al., Transition metal-engineered magnesium-based materials for advanced hydrogen storage: From multifaceted mechanisms to state-of-the-art systems, J. Environ. Chem. Eng. 13 (1) (2025) 115109.
[70] J. Zhang, M. Liu, J. Qi, et al., Advanced Mg-based materials for energy storage: fundamental, progresses, challenges and perspectives, Prog. Mater. Sci. 148 (2025) 101381.
[71] V.N. Kudiiarov, N. Kurdyumov, R.R. Elman, et al., Microstructure and hydrogen storage properties of MgH_2/MIL-101(Cr) composite, J. Alloys Compd. 976 (2024) 173093.
[72] J.S. Blázquez, F.J. Romero, C.F. Conde, et al., A review of different models derived from classical Kolmogorov, Johnson and Mehl, and Avrami (KJMA) theory to recover physical meaning in solid-state transformations, Phys. Status Solidi (B) Basic Res. 259 (6) (2022) 2100524.
[73] T. Huang, C. Zhou, Surface diffusion-controlled Jonhson-Mehl-Avrami-Kolmogorov model for hydrogenation of Mg-based alloys, J. Phys. Chem. C 127 (2023) 13900–13910.
[74] T. Huang, H. Liu, C. Zhou, Effect of driving force on the activation energies for dehydrogenation and hydrogenation of catalyzed MgH_2, Int. J. Hydrogen Energy 46 (2021) 37986–37994.
[75] Y. Huang, C. An, Y. Liu, et al., Unraveling the kinetic mechanism of atomic hybrids for the catalytic dehydrogenation of MgH_2, J. Mater. Sci. Technol. 212 (2025) 89–95.
[76] S. Li, P. Jen, Dehydrogenation mechanism in catalyst-activated MgH_2, Phys. Rev. B 74 (2006) 132106.
[77] J. Tang, X. Yang, L. Chen, et al., Modeling and stabilities of Mg/MgH_2 interfaces: a first principles investigation, AIP Adv. 4 (2014) 077101.
[78] A. Surrey, L. Schultz, B. Rellinghaus, Electron beam induced dehydrogenation of MgH_2 studied by VEELS, Adv. Struct. Chem. Imaging 2 (2016) 7.
[79] M.V. Antisari, A. Aurora, D.M. Gattia, et al., On the nucleation step in the Mg-MgH_2 phase transformation, Scripta Mater. 61 (2009) 1064–1067.
[80] N. Skryabina, V. Aptukov, D. Fruchart, Role of induced elastic deformations at the Mg/MgH_2 transformation, J. Alloys Metall. Syst. 5 (2024) 100064.
[81] K. Nogita, X.Q. Tran, T. Yamamoto, et al., Evidence of the hydrogen release mechanism in bulk MgH_2, Sci. Rep. 5 (2015) 8450.
[82] O. Friedrichs, F. Aguey-Zinsou, J.R. Fernandez, et al., MgH_2 with Nb_2O_5 as additive, for hydrogen storage: chemical, structural and kinetic behavior with heating, Acta Mater. 54 (2006) 105–110.
[83] L. Ren, Y. Li, Z. Li, et al., Boosting hydrogen storage performance of MgH2 by oxygen vacancy-rich H-V2O5 nanosheet as an excited H-pump, Nano-Micro Lett. 16 (2024) 160.

[84] C. Li, Y. Ding, X. Zhang, et al., Hydrogen storage in magnesium hydride at room temperature enabled by graphene-stabilized multivalent niobium oxides, Adv. Mater. 37 (2025) e11759.
[85] A. Perejon, P.E. Sanchez-Jimenez, J.M. Criado, et al., Magnesium hydride for energy storage applications: the kinetics of dehydrogenation under different working conditions, J. Alloys Compd. 681 (2016) 571–579.
[86] M. Antisari, A. Montone, A. Aurora, et al., Scanning electron microscopy of partially de-hydrogenated MgH_2 powders, Intermetallics 17 (2009) 596–602.
[87] X. Zuo, X. Mo, W. Zhou, et al., Enhanced dehydrogenation of MgH_2 modified by Ti and S: a first-principles investigation, Int. J. Hydrogen Energy 83 (2024) 1309–1319.
[88] S.T. Sabitu, A.J. Goudy, Dehydrogenation kinetics and modeling studies of MgH_2 enhanced by NbF_5 catalyst using constant pressure thermodynamic forces, Int. J. Hydrogen Energy 37 (2012) 12301–12306.
[89] S.T. Sabitu, O. Fagbami, A.J. Goudy, Kinetics and modeling study of magnesium hydride with various additives at constant pressure thermodynamic driving forces, J. Alloys Compd. 509S (2011) S588–S591.
[90] S.T. Sabitu, A.J. Goudy, Dehydrogenation kinetics and modeling studies of MgH_2 enhanced by transition metal oxide catalysts using constant pressure thermodynamic driving forces, Metals 2 (2012) 219–228.
[91] Y. Li, Y. Zhao, S. Cao, et al., Study on mechanisms of two-step hydrogen sorption in a MgH_2-TiCrMnFeZr high-entropy alloy composite, J. Mater. Chem. A 13 (2015) 23632.
[92] H. Lu, J. Li, K. Nie, et al., Single-atom Cu supported on Ti3C2Tx for catalyzing hydrogen storage in MgH2, J. Phys. Chem. Lett. 16 (2015) 3525–3534.
[93] Y. Chrafih, R.T. Alqahtani, A. Ajbar, et al., Multi-scale modeling of doped magnesium hydride nanomaterials for hydrogen storage applications, Nanomaterials 15 (2025) 1470.
[94] J.F. Fernandez, C.R. Sanchez, Rate determining step in the absorption and desorption of hydrogen by magnesium, J. Alloys Compd. 340 (2002) 189–198.
[95] J. Cermak, L. Kra, Hydrogen diffusion in Mg-H and Mg-Ni-H alloys, Acta Mater. 56 (2008) 2677–2686.
[96] E. Evard, I. Gabis, V.A. Yartys, Kinetics of hydrogen evolution from MgH_2: experimental studies, mechanism and modelling, Int. J. Hydrogen Energy 35 (2010) 9060–9069.
[97] Y. Li, Z. Ding, H. Jiang, et al., Spatially programmed confinement catalysis enables high performance magnesium hydrogen storage, Nano Lett. 25 (48) (2025) 16801–16808.
[98] Y. Ye, Z. Zhang, J. Liu, et al., Experiment and simulation study on transfer phenomena and performance optimization of MgH_2 based hydrogen storage reactors, Int. J. Hydrogen Energy 86 (2024) 649–661.
[99] D.A. Lanbaran, C. Wang, C. Wen, et al., Modeling the impact of temperature-dependent thermal conductivity on hydrogen desorption from magnesium hydride, Int. J. Hydrogen Energy 138 (2025) 491–508.
[100] Z. Gao, X. Yang, Z. Zhuang, et al., Catalytic strategies and mechanisms for enhancing MgH_2 solid-state hydrogen storage, Chem. Catal. 6 (2026) 101692.